Magnetic Resonance Imaging, Vol. 17, No. 10, pp. 1457–1468, 1999
© 1999 Elsevier Science Inc. All rights reserved.
Printed in the USA.
0730-725X/99 $–see front matter

PII S0730-725X(99)00098-3

● *Original Contribution*

HIGH-RESOLUTION IMAGING USING HADAMARD ENCODING

DOUGLAS W. FLETCHER,* JOHN C. HASELGROVE,† AND LIZANN BOLINGER‡

*Department of Biochemistry and Biophysics, University of Pennsylvania, Philadelphia, PA, 19104 USA; †Department of Radiology, Children's Hospital of Philadelphia, Philadelphia, Pennsylvania, 19104; and ‡University of Iowa, Department of Radiology, Iowa City, IA 52242-1009, USA

High-resolution imaging techniques using noninvasive modalities such as magnetic resonance (MR) imaging are being pursued as in vivo cancer screening techniques in an attempt to eliminate the invasive nature of surgical biopsy. When acquiring high-resolution MR images for tissue screening, image fields of view have in the past been limited by the matrix sizes available in conventional MR scanners. We present here a technique that uses aliasing to produce high resolution images with larger matrix sizes than are currently available. The image is allowed to alias in both the frequency encoding and phase encoding dimensions, and the individual, aliased fields of view are recovered by Hadamard encoding methods. These fields may then be tiled to obtain a composite image with high spatial resolution and a large field of view. The technique is demonstrated using two-dimensional and three-dimensional in vivo imaging of the human brain and breast. **© 1999 Elsevier Science Inc.**

Keywords: **High-resolution imaging; Hadamard.**

INTRODUCTION

In situations where high resolution is required for in vivo tissue screening, it is possible that the matrix size available on the scanner may limit the field-of-view (FOV). As a result current high-resolution tissue screening techniques using MRI necessitate either a priori knowledge of lesion position or the acquisition of multiple single–voxel images to cover the large FOV. In cases where either multiple lesions exist or a priori knowledge of lesion position is absent, imaging a restricted FOV[1,2] may result in vital information being lost.

We have developed a technique that uses Hadamard encoding to allow high-resolution imaging over an extended FOV. Multiple small images are acquired and these images are then combined by tiling to form a high–resolution image with a large FOV, but the signal-to-noise ratio (SNR) is greater than conventional tiling techniques. Hadamard encoding has been used in NMR spectroscopy and imaging to allow the acquisition of signals from spatially distinct regions of tissue.[3–10] Previously, when Hadamard and Fourier encoding have been used together they have been used to encode perpendicular spatial directions. However, because Hadamard and Fourier encoding schemes are both linear operations, they can be applied co-linearly to increase the in-plane FOV of an image obtained with high spatial resolution. Hadamard encoding of either the longitudinal or transverse magnetization is performed within the plane of the image by using Walsh functions that divide an object into various regions of interest. Walsh functions have values of only $+1$ and -1, and form an orthogonal set; each particular function is defined by its 'sequency' which is the number of times the function reverses sign as shown in Fig. 1. Once encoded, these regions are allowed to alias onto one another; the separate regions are reconstructed by means of a Hadamard transform. Because information is acquired about the entire region of interest simultaneously, this technique allows a SNR per unit time increase of $\sqrt{N}$, where N is the order of the Hadarmard encoding matrix, over acquiring the same region of interest with multiple smaller regions of interest. Although the general strategy for the spatial encoding and decoding is the same for two- and three-dimensional imaging, there are differences in the practical applications. We here discuss first the Had-

RECEIVED 8/15/98; ACCEPTED 8/8/99.
Address correspondence to: Douglas W. Fletcher, Ph.D., Department of Radiology, National Naval Medical Center, 8901 Wisconsin Ave., Bethesda, Maryland 20889. Tel: (301) 319-4488; Fax: (301) 295-5788; E-mail: fletcher@bethrad.med.navy.mil

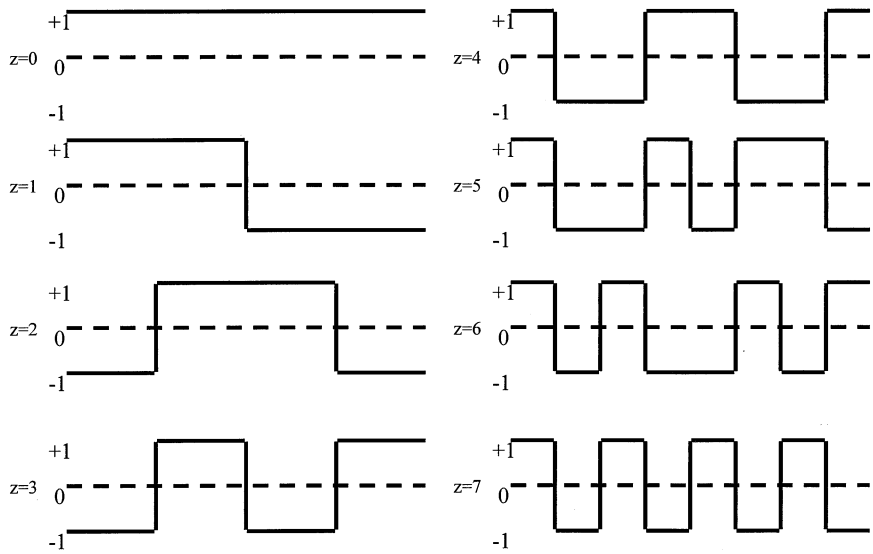

Fig. 1. Walsh functions. The Walsh functions show the frequency profile that the Hadamard pulses must produce during the pre-encoding. These functions make up a complete orthogonal set. Walsh functions are described by sequency that is similar to the concept of frequency but indicates the number of zero crossings. The sequency for the functions illustrated in this figure are indicated by the letter z.

amard encoding scheme for two-dimensional images, and then describe the application for three dimensions.

METHODS

Description of Hadamard Encoding

The general strategy of Hadamard encoding is to allow the signals (Si) from the different regions to combine to generate a single detected signal (Sd) as explained in Bolinger et al.[3] To resolve ′N′ distinct regions, N separate signals (Sd) are acquired, but for each one, the phases of the components (Si) are varied from acquisition to acquisition. The N signals (Sd) are then combined by simple addition and subtraction in a fashion dictated by the Hadamard decoding scheme to generate the individual signals (Si) from the N independent regions. An example of a 2 × 2 decoding scheme is shown in Fig. 2.

Data are acquired using a pulse sequence that will generate an image with the required high resolution: the FOV of this image (which we call the image field-of-view: FOVi) is defined by the maximum permissible matrix size. We assume that FOVi is less than the total FOV of interest (we call this the composite field-of-view: FOVc), and that FOVc is larger than FOVi by a factor of N in the read direction and by M in the phase direction. By selecting the width of the acquisition filter to be that of FOVc, the N × M separate regions will alias onto a single image. We call these separate regions tiles. Each pixel in the composite aliased image will then have an intensity that is a sum of the corresponding pixels in the N × M separate tiles, the phases of which are controlled using spatial encoding schemes dictated by Walsh functions. N × M separate images are then acquired with N × M different Walsh function combinations, and these images are decoded by using Hadamard decoding to generate N × M separate images, one for each tile, that can then be combined to generate a composite image.

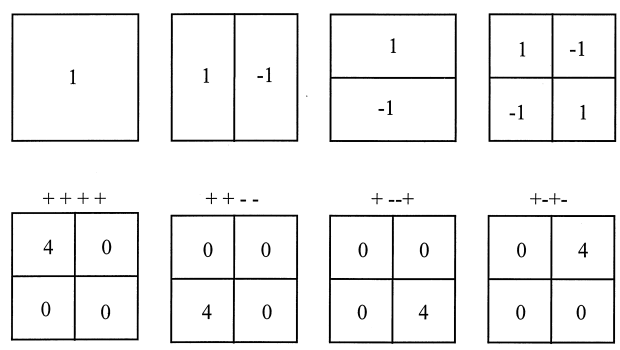

Fig. 2. Encoding scheme for 2*2 Hadamard encoded images. Demonstration of an idealized 2*2 Hadamard encoding scheme and resulting reconstructed images. The top row is the four encodings with resultant relative signal. The encoding pulses yield 180° flips. The bottom row is the four reconstructed images from the experiment with the decoding used labeled above each image.

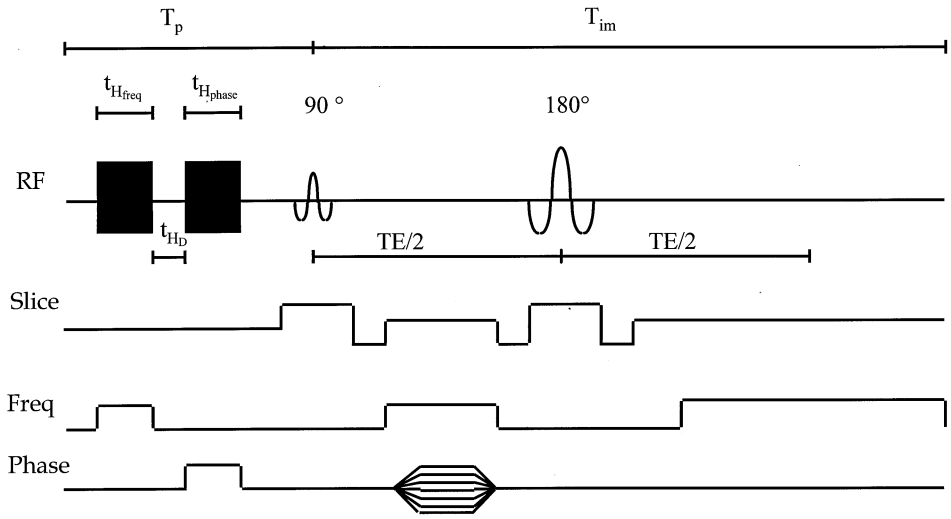

Fig. 3. Hadamard multivolume imaging pulse sequence. The Hadamard multivolume imaging pulse sequence contains two independent sections, the pre-encoding section of length T_p and the imaging section of length T_{im}. Hadamard pre-encoding provides additional encoding of regions of interest within the plane of the image. The imaging section may contain any imaging pulse sequence. Here we have shown a spin echo sequence. To encode the multiple volumes of interest, N × M images must be acquired utilizing all of the Hadamard pulses in each direction and in all combinations. The FOV of the imaging sequence is set to the FOV of the region of interest and the image is allowed to alias. Decoding using the Hadamard scheme produces N × M images at the small FOV that may be tiled together to provide the large FOV image.

Two-Dimensional Imaging

Figure 3 is a schematic of the pulse sequence for two-dimensional Hadamard encoded imaging. It has two separate sections, (1) spatial pre-encoding, T_p (2) the imaging section, T_{im}.

1. The pre-encoding section performs the spatial encoding successively in the phase and frequency directions by applying r.f. pulses in the presence of gradients to modify the longitudinal magnetization. The r.f. pulses each have an excitation profile that matches one of the Walsh excitation profiles that can be generated either by using multiband inversion pulses[3,4] or by applying a single-band inversion pulse multiple times. We have used both methods.
2. Any imaging sequence can be used. The imaging parameters (FOV, matrix size, and bandwidth) are designed to meet the requirements described above. As an example, we have shown a simple spin echo sequence in Fig. 3.

Images of phantoms were obtained on a custom-built spectrometer interfaced to a 2T Oxford, whole-body magnet. A cosine coil[11] tuned to 86 MHz provided homogeneous B_1 excitation across the phantom, which consisted of two glass tubes containing 1 mM $CuSO_4$ for which T_1 and T_2 values were equal: about one second. A simple spin echo sequence (TR/TE = 2000/25 ms) was used after Hadamard pre-encoding (see Fig. 1). Non-aliased images were acquired with parameters: FOV = 10 cm, TH = 10 mm, sampling rate = 25 kHz, the analog filter = 25 kHz. Aliased images were acquired with FOV = 5 cm image, TH = 10 mm, sampling rate = 25 kHz, the analog filter = 50 kHz. For both data sets the data acquisition matrix size was 256 × 128 and the final image was interpolated to 256 × 256. Each Walsh function pulse was a Shinnar–LeRoux pulse[12–14] 4 ms in length with a delay of 2 ms between the last pulse and the excitation pulse of the imaging sequence. Five milliseconds separated the centers of the two Walsh function pulses.

Images of a human brain were obtained on a Siemens 1.5T VISION system using a standard quadrature head coil. The multiband (Walsh function) inversions for the Hadamard pre-encoding scheme were performed using multiple Silver–Hoult adiabatic inversion pulses[15,16] with μ of 10 and a β of 87.56 s as shown in Figure 4. Although this lengthened the pre-encoding time to 28.5 ms, it eliminated both the effects of B_1 inhomogeneity and the ripples that were evident in the phantom images due to the r.f. profile when using the Shinnar–LeRoux pulses. The image was acquired using a turbo spin echo imaging sequence with parameters: TR/TE = 2000/120 ms, echo train length of 15, image FOV = 6 cm, TH = 5 mm and composite FOV = 24 cm. The acquisition

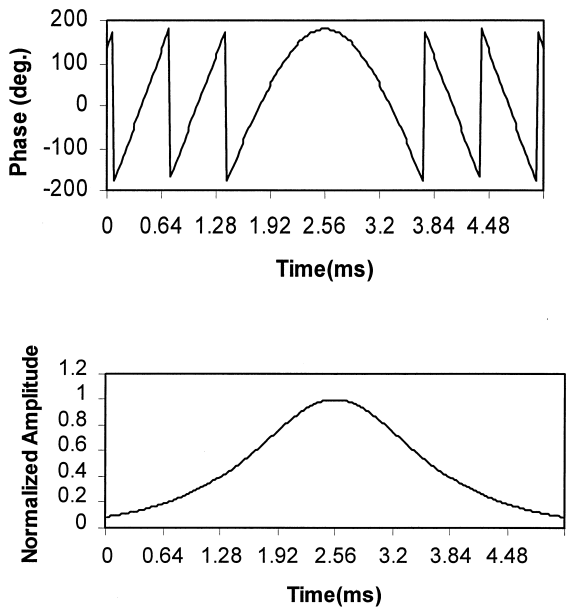

Fig. 4. Example of a hyperbolic secant pulse. A hyperbolic secant pulse plotted as an amplitude and phase modulated RF pulse with $\mu = 10$ and $\beta = 87.54$ Hz.

matrix was 180 × 256, interpolated to 256 × 256. Thus, the resulting composite image had an equivalent matrix size of 1024 × 1024. Siemens scanners are able to acquire images with 1024 matrix, but we chose these values to demonstrate the technique. It is expected that in practice, the matrix size of the composite image will be larger than the maximum available on the scanner.

Three-Dimensional Imaging

Hadamard encoding can also be applied to increase the fields of view in the phase and frequency directions of a three-dimensional image set. The encoding scheme is slightly different from the two-dimensional case to avoid the saturation of the encoding longitudinal magnetization that would result from the short TR times used in three-dimensional imaging. For three-dimensional imaging, the encoding uses the transverse magnetization[17] and is performed using the excitation pulse of the imaging sequence (Fig. 5). One Hadamard encoding would be applied for every TR with 16 echoes per TR. Instead of encoding with or without an inversion pulse before each TR, one of two 30° pulses are used. Figure 6 shows two pulses used to create the desired excitation profiles. The first is a single sinc pulse yielding a 30° excitation–profile. The second is a composite of two sinc pulses phase shifted with their resultant excitation response. These two sinc pulses yield two pass bands that have identical profile amplitudes but are 180° out of phase from one another. In the linear regime, i.e., low flip angle, the sinc pulse response is very stable. The truncation artifacts resulting from limited pulse application time are unavoidable. However, the profiles yield satisfactory results when encoding pulses of +30° and −30° were used.

In the two-dimensional encoding experiment, the different encodings had differing times that the longitudinal magnetization would be relaxing. This time could vary from 0 ms to 28.5 ms for the 4 × 4 encoding scheme. This additional time results in the separate Hadamard encoded images to no longer be normalized. Upon re-

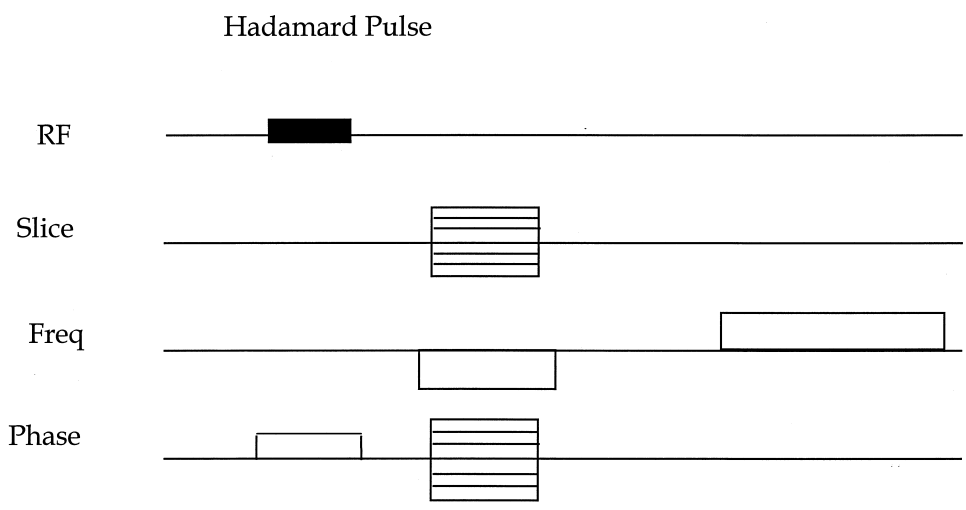

Fig. 5. Three-dimensional Hadamard encoded multi-slice sequence. A conventional three-dimensional sequence with the slab select pulse replaced by a Hadamard pulse. Unlike the earlier sequences, there are no longer two sections and the Hadamard pulse is applied in place of the slab select pulse during each TR.

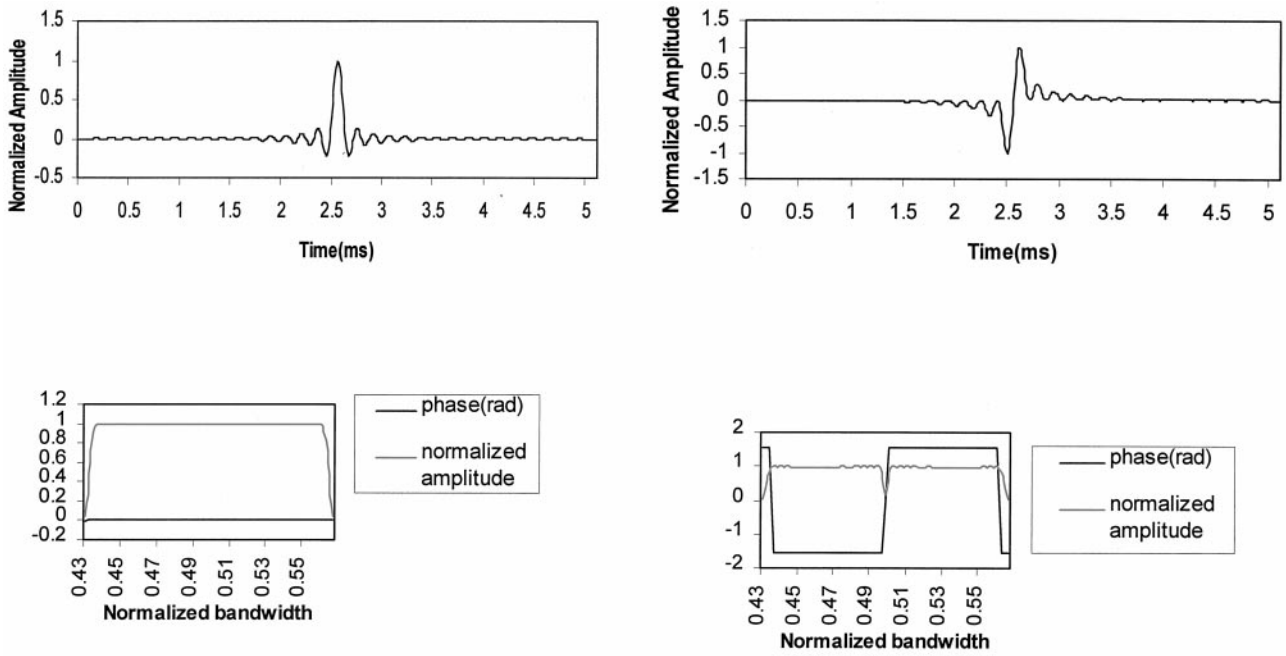

Fig. 6. Hadamard encoding pulses for 3D sequence. Multiple sinc pulse shapes (top) and the excitation responses for 30° flip angle (bottom). The left is a single sinc pulse and its resultant excitation profile. The right is sinc pulses that are phase shifted from one another. The resultant excitation profile has uniform amplitude in the two regions but they are 180° out of phase from one another.

construction, these unnormalized images can result in significant reconstruction errors. Regions that are encoded with 30° and −30° multiple sinc pulses both reach the same steady state value. In comparison with the first experiment, these low flip angle Hadamard encoding pulses result in regions with identical longitudinal magnetization. Thus, these regions can be reconstructed without significant errors using the Hadamard decoding process.

Human breast images were acquired using a 1 × 2 Hadamard encoding scheme on a 4T Signa scanner (GE Medical Systems, Milwaukee, WI, USA). A three-dimensional fast gradient echo sequence was modified to apply Hadamard encoding in the phase direction using multiple low-angle sinc pulses in place of the usual slab selection pulse. Two images were acquired: one with a zero sequency encoding profile, the other with sequency equal to one.[8] The use of the slab excitation pulse for Hadamard encoding instead of slab selection forces the use of a FOV in this direction that is larger than the object being imaged to prevent unwanted aliasing in that direction. A biplanar coil[18] was used to excite the spins and a four-coil array[19] was used to receive the signal. Twenty-eight adjacent sagittal slices were selected to cover the entire breast (TR: 17.7 ms, TE: 5.9 ms, TH: 2 mm, MAT: 256*128, FOV: 8*8 cm). The time of acquisition for the Hadamard encoding three-dimensional sequence is approximately 12 s greater than the conventional three-dimensional fast gradient echo sequence time of 60 s. This increase in time over the product version of the FGRE3D sequence is largely caused by the replacement of the slab select pulse of 3.2 ms pulsewidth with the low angle sinc pulse of pulsewidth 5.12 ms. A pulsewidth of 5.12 ms was chosen for the pulse to ensure that peak B1 was within the limits of available RF.

RESULTS

Two-Dimensional Imaging

Figure 7 demonstrates the effect of the Hadamard encoding when no aliasing is allowed, and Fig. 8 shows the effect of combining the Hadamard encoding and aliasing.

Figure 7 shows images of a phantom consisting of two tubes placed perpendicular to each other so that one looks like a rectangle while the other like a circle. The FOV of 10 cm is large enough to cover the entire phantom. There is a unique mapping of each point in the image to each voxel in the object. Figure 7A shows the image acquired with the Walsh function with zero sequency. For zero sequency all points have positive phase, and the image is a conventional image. Figure 7B shows the same sample when the Hadamard pre-encoding inverted the top part of the FOV. The symbols underneath the image indicate the sign of the signal in the image in

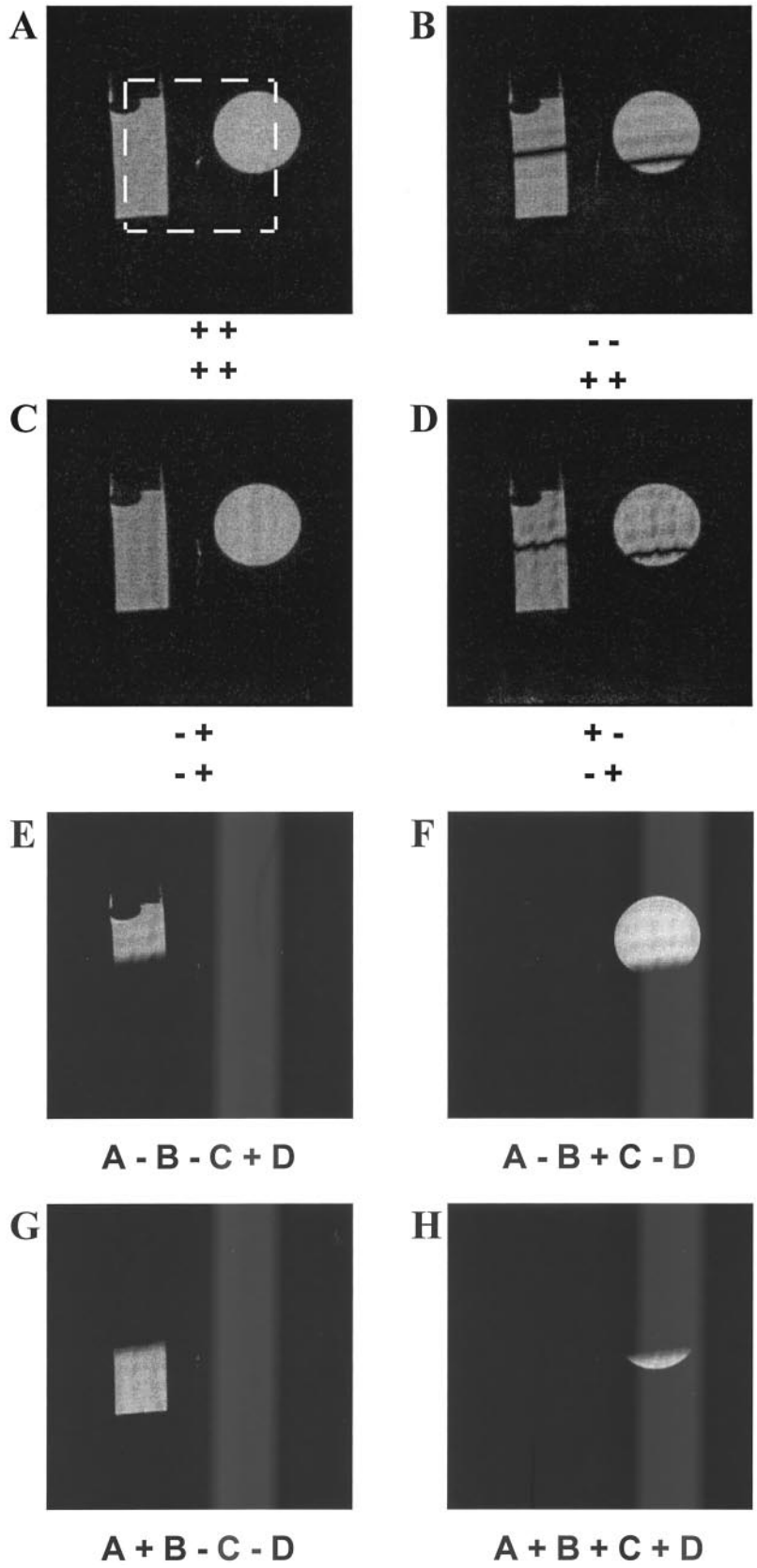

Fig. 7. Example of Hadamard multivolume imaging scheme. The images of the phantom were acquired with a spin echo sequence with TR/TE of 2000/25 ms, TH of 10 mm and a FOV of 10 cm. A second order Hadamard encoding was performed within the plane of the image. A–D are the images that resulted from the four Hadamard encodings. A has no inversion pulse. The dashed white line shows the image FOV of Figure 8. B has an inversion pulse applied to the top half of the image, i.e., in the y direction. C has an inversion pulse applied to the left half of the image and D has inversion pulses applied in both the top half and the left half. The encoding matrix for each image is shown directly below it. The images in E–H resulted from decoding the Hadamard encoding. The equation below each image shows how the raw data from images A–D were combined to attain these images.

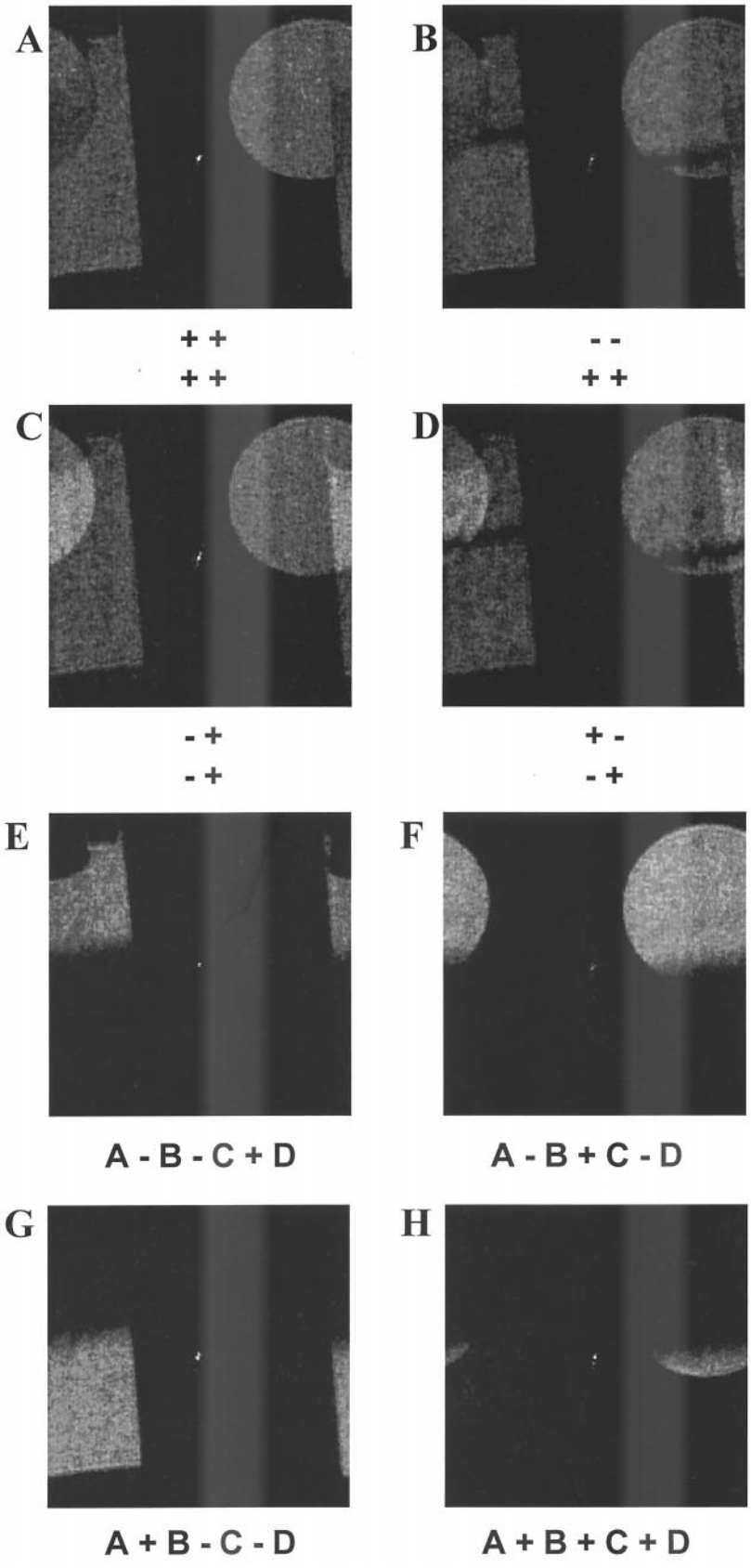

Fig. 8. Example of Hadamard multivolume imaging with aliasing. Figure 8 is the same as Figure 7 except that the data were acquired with gradient strengths equivalent to a 5-cm FOV. The resulting aliased images are evident in the Hadamard encoded images in A–D. That FOV is shown as a dashed white line in Figure 7A. By using a Hadamard encoding/decoding scheme we are able to separate the individual aliased component that are images shown in E–H. If unwrapped, these images could be tiled to result in a 10-cm FOV image at the 5-cm resolution. In addition, each of the 5-cm images has the signal-to-noise of a single 5-cm FOV image with 4-signal averages.

each of the 4 quadrants. The image is displayed as a conventional magnitude image, so both the upper (inverted) and lower (noninverted) part of the image appear bright. One can see a line in the image where the inversion pre-encoding pulse makes a transition from inversion to non-inversion. Because this line follows isocontours of B_0, it does not go exactly across the image because of field inhomogeneities. Furthermore, the excitation profile of the inversion pulse has approximately a 15% ripple that is visible in the image. Figure 7C is similar to Fig. 7B except that the left side of the image (rather than the top) was inverted. The line separating the inverted and non-inverted regions falls between the circle and the rectangle and is indistinguishable from the background. Figure 7D is the image of the phantom when two successive inversion pulses have been applied: the top was inverted, and then the left of the image inverted. The lower right hand quadrant has been inverted twice, and has therefore effectively not been changed, as indicated by the symbols underneath the image. The ripple and the black line demarcating the inverted and non-inverted regions are again visible.

Figures 7E–H show the images obtained when the raw component images (7A–D) are combined by addition and subtraction using the Hadamard decoding scheme listed beneath each image. For example, if we sum images B and C and subtract the result from the sum of images A and D, (A−B−C+D) then the signals in all but the top left hand quadrant cancel as shown in Figure 7E. The results of other linear combinations are shown in Fig. 7F–H. Thus from 4 images in which the separate quadrants have varying signs, we can reconstitute 4 images each containing *only* the signal from one of the quadrants.

Figure 8 shows the application of the Hadamard encoding scheme to the same phantom as in Fig. 7, but the FOV is reduced so that the edges of the total composite FOV are allowed to alias on top of each other. The dashed line on Figure 7A shows the FOV of the image of Fig. 8. Figure 8A is the basic image with a 5-cm image FOV; the center of this FOV corresponds to the center of the FOV of Fig. 7. Figures 8B–D show the effects of using the alternate Walsh encoding. Figures 8E–H are analogous to Figure 7E–H and show the effects of appropriate Hadamard decoding to generate the signal from each tile.

This use of the Hadamard encoding for imaging is easiest to understand when the zero crossing points of the Walsh functions occur at the edges of the imaging 'tiles'. However this is not a prerequisite of the technique; the requirement is that the basic small area of the Walsh functions is the same size and shape as the individual image tiles. Practical application is easiest when the small image is centered in the FOV of the large image, but with the Walsh zero crossings referenced from the center of this image—as shown in Fig. 7. This offset has the result that the individual tiles derived from the Hadamard decoding are all offset in each direction by half of the FOV, as seen in Fig. 8. The final composite image is then generated by shifting the image of each tile before combining. The final results of such manipulation can be seen in the 4 × 4 Hadamard image of a human brain shown in Fig. 9. The resulting in plane resolution is 220 by 330 μm.

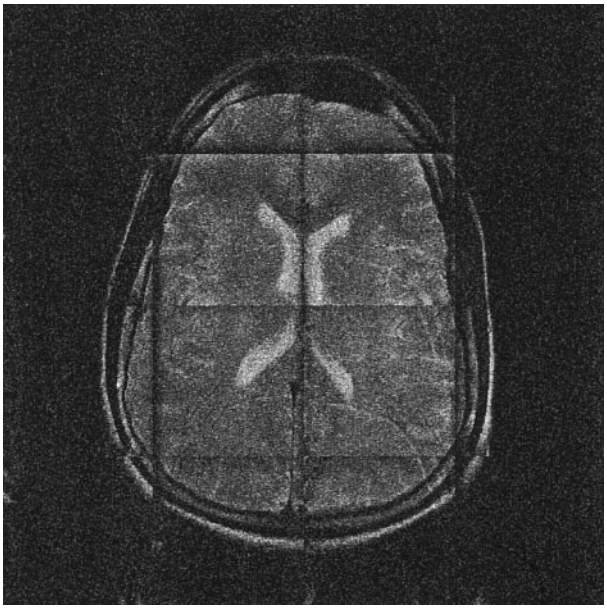

Fig. 9. 4 × 4 Hadamard encoded brain image. The image of this brain was acquired using a 4 × 4 Hadamard scheme followed by a turbo fast spin echo–imaging scheme. The resulting 16 images of FOV 6 cm were Hadamard decoded, unwrapped and then tiled to give the resulting 24 cm composite FOV image.

Three-Dimensional Imaging

Three-dimensional imaging of a human breast was performed using a 1 × 2 Hadamard encoding matrix in combination with a 28-slice three-dimensional imaging sequence. The two sagittal image sets were obtained with sequency 0 and 1 were both added and subtracted to reconstruct the two encoded regions for each slice. Four slices from this data set are displayed in Fig. 10. If we allow the readout direction to be placed in the shorter dimension and the phase and Hadamard encoding to be performed in the longer dimension one can see that a 1*2 Hadamard matrix can be ideal. A digital filter exists in the readout direction but does not exist in the phase encoding direction. Therefore, if the object is larger than the FOV in the phase encoding direction, aliasing will occur. One way to eliminate the effects of aliasing with

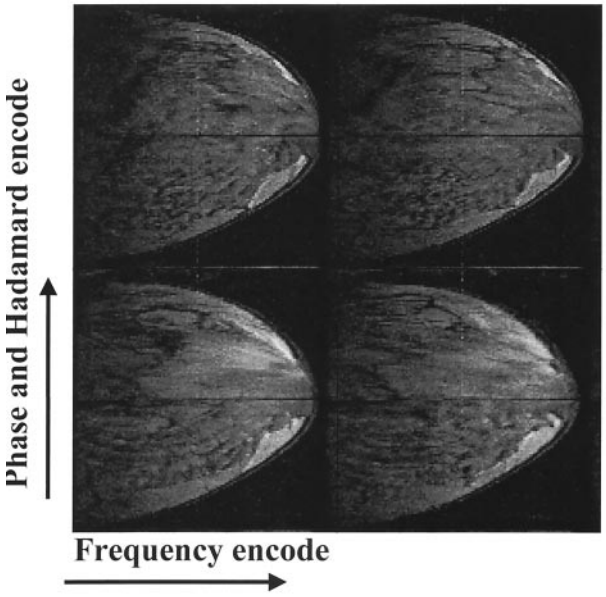

Fig. 10. Reconstructed images of a human breast using a 1*2 Hadamard encoded multi-slice sequence. Four Reconstructed sagittal images of a human breast from a 1*2 Hadamard encoded multi-slice sequence. 28 adjacent sagittal slices were selected to cover the entire breast tissue of which 16 images are shown above (TR: 17.7 ms, TE: 5.9 ms, TH: 2 mm, MAT: 256*128, FOV: 8*8 cm). Each image is a composite of two Hadamard images. Therefore, the individual slices are displayed with a FOV of 8 × 16 cm and a composite matrix size of 512 × 256. Hadamard, phase, and frequency encoding directions are displayed.

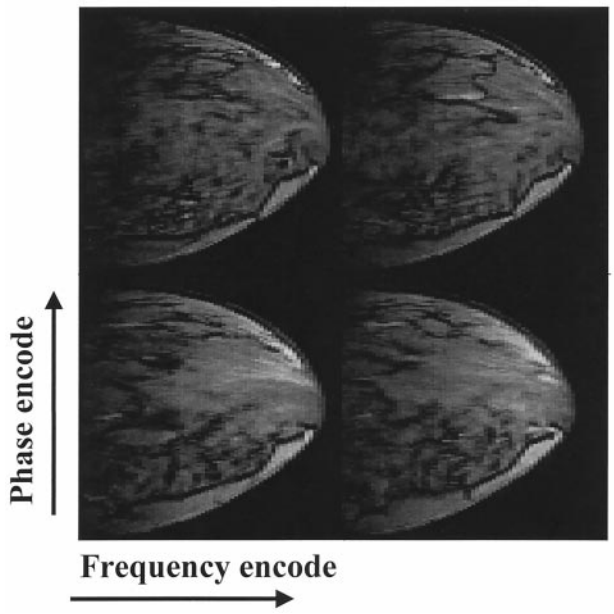

Fig. 11. Reconstructed images of a human breast using a conventional three-dimensional fast gradient echo sequence. Four images of a human breast acquired using a conventional sagittal 3DFGRE sequence. 28 adjacent sagittal slices were selected to cover the entire breast tissue of which 16 images are shown above (TR: 14.9 ms, TE: 5.9 ms, TH: 2 mm, MAT: 256*128, FOV: 16*16 cm). These images are of the same breast as Fig. 10.

conventional imaging is to oversample. Oversampling involves collecting twice the amount of lines necessary in a direction and discarding the information on the edges. Oversampling is usually performed in the readout direction. However, in our case, we are going to oversample in the phase encoding direction. Many clinical scanners perform this function to allow high–resolution acquisitions. This doubles the experiment time without yielding an increase in information. Hadamard encoded imaging insures that all the information that is collected will be useful in reconstructing the image and no information is discarded. Another possibility would be to reverse the phase encoding and readout directions, which would allow the acquisition of the same data in half the time due to requiring only half the number of phase encodes. Unfortunately, this direction is the same direction as the chest wall. If we were to place the phase encoding along this direction, the chest wall and body would alias into the image. By placing the readout direction in this dimension instead of the phase encoding, we utilize the readout filters available on most scanners and ensure that the chest wall will not alias into the image. If we align the encoding matrix so the longer dimension corresponds to the longer dimension of a sagittal image of a human breast in the bilateral cosine coil, one can see that the shape of the breast and the encoding matrix align well. If we now shorten the FOV in the phase encoding direction to equal that of the readout direction, an image aliased only in the phase encoding direction will result.

The individual FOVi are each 8 × 8 cm and the matrices 256 × 128, giving a pixel size of 0.312 × 0.625 mm. Each image is the composite of two Hadamard images. Therefore, the individual slices are displayed with a FOV of 8 × 16 cm and a composite matrix size of 512 × 256. For comparison, Fig. 11 shows the same slices of the same breast tissue acquired with a conventional three-dimensional fast gradient echo sequence. The FOV and matrix sizes are 16 cm and 256 × 128, giving a pixel size of 0.625 × 1.25 mm which is twice that of the image in Fig. 10. In this study, we neither added contrast medium nor employed FATSAT, so the images seem slightly different than conventional clinical images. The images seem very similar, but the higher resolution of the Hadamard image (Fig. 10) is, as expected, accompanied by a reduced SNR.

Table 1.

	Nphase	Nfreq	bw/pixel	S:N for each image	Time (× TR) for each image	No. of images	Rel S:N of final image	Rel time of final image
Single high resolution image	M*Np	N*Nf	Bp	√ (M*Np/BP)	M*NP	1	√M	M
Local areas—for tiling	Np	Nf	Bp	√ (Np/Bp)	Np	1	1	1
Simple composite					N*M*Np	N*M	1	N*M
Single H acq (as 1)	Np	Nf	N*BP	√ (Np/(N*Bp))	Np	1	1/√N	1
Tiling with the above					N*M*Np	N*M	√M	N*M

SNR Comparison

The encoding process we describe here sums (with varying phase) ′N′ images to reconstruct a series of ′N′ tiles, so we expect each tile of the reconstructed Hadamard image to have a SNR factor of $\sqrt{N}$ larger than the SHR of the component images. The advantage of the Hadamard technique may be seen clearly by reference to Table 1, where we compare the time taken and the signal-to-noise of three different approaches to acquiring given FOV with a defined pixel size.

We use the following terms:

Np,Nf = acquistion matrix in the phase and frequency directly.
Bp = bandwidth/pixel.

The signal-to-noise of each separate image is then given by the relation:

$$S{:}N \ \alpha \ \sqrt{(Np/Bp)}$$

The different techniques are:

1. A single image in which the matrix is high enough that the required resolution is achievable. This is our reference.
2. The conventional tiling approach in which N * M separate images are acquired, each with a FOV of 1/N (in the frequency direction) and 1/M (in the phase direction) of the required large FOV. The signal-to-noise of each of these tiles is the same as for the single large image, but they take M × longer to acquire.
3. The Hadamard approach in which N × M small images are acquired. Each individual image has the same signal-to-noise as the individual image of technique 2, but the Hadamard decomposition improves the signal-to-noise by a factor of $\sqrt{M}$. Thus, although these images take M × longer to acquire than the single large image, the signal-to-noise is $\sqrt{M}$ better.

The message from this analysis is clear. If the required image can be acquired in a single pass, then that is the appropriate manner in which to do so. However, if the combination of available matrix size and resolution do not allow the required FOV to be imaged in one pass, then Hadamard imaging allows the data to be acquired in the same time needed for the conventional tiling approach, but provides an increase of $\sqrt{M}$ in signal : noise. These arguments hold true even if the region of interest is a subregion of the subject—for example, if it is necessary to image one hemisphere of a brain with ultra–high resolution. Whenever multiple images of contiguous regions need to be acquired, the use of Hadamard encoding allows for an increase in signal:noise without an increase in acquisition time.

We compared the SNR in the two-dimensional images of Fig. 8, where N had a value of 4 and where we would expect a SNR increase by a factor of 2. Two regions were chosen (one within each phantom) and the average values were used as the signal. A region outside of both phantoms was chosen and its average value was used as the noise in the following ratios. For the circular phantom, the measured values for SNR were 2.06 in Fig. 7E and 3.78 in Fig. 8F indicating an increase of 1.83 in signal-to-noise. For the rectangular phantom, S:N measurements of 1.91 and 3.23 for Figures 7F and 8F respectively, show that the Hadamard reconstruction increased the SNR by a factor of 1.69. These SNR increases are both within 15% of the predicted value of 2. We would expect some variation in the SNR increase due to experimental and machine error so we feel that the theoretical increases brought about by Hadamard encoding in two dimensions are supported by experimental results.

To compare the SNR of three-dimensional images directly we acquired two in vivo image sets of a human breast in which both the standard image and the 1 × 2 Hadamard image had the same voxel dimensions. For both images the breast fit completely within the chosen FOV (16-cm) and all acquisition parameters remained constant. No aliasing occurred in either experiment, so in this respect the Hadamard reconstruction was similar to that shown in Fig. 7. For this measurement we acquired the two component images of the Hadamard images with

NEX = 1, and acquired the conventional image with NEX = 2. We expected to generate two images with similar signal-to-noise. No aliasing occurred in the experiment, and we purposefully acquired the conventional image with a NEX of 2 to equate the SNR increase brought about by the Hadamard image. A region of interest within the breast tissue was chosen for measuring the signal, and another outside the tissue was chosen as background. The Hadamard image yielded a SNR of 80.1 whereas the conventional imaging sequence yielded a SNR of 79.2. Thus the signal-to-noise behavior is as expected. The required increase in NEX of the conventional images to match that of the Hadamard images would need to be performed for each smaller FOV image. To get the identical SNR value for a 1×2 Matrix in the phase encoding direction, 2 NEX are required. To get the identical SNR value for a 1×4 Matrix in the phase encoding direction, 16 NEX are required. Therefore one can see that a great time advantage is gained in this direction using Hadamard encoding.

One should keep in mind that clinically the resolution of these images would be increased by at least a factor of two. This higher resolution would require the traditional image to be acquired with "no phase wrap" so that aliasing would not be introduced into the image. This is accomplished by acquiring twice the amount of lines in the phase encoding direction and discarding this information. To acquire the entire region of interest, two separate images would be required. In this case, the time required to image the breast would be identical to that required by the Hadamard encoding procedure. However, as the above argument states, the Hadamard encoding acquired information from the entire object simultaneously on both image acquisitions and thus would allow an SNR factor increase of 1.41 over the multiple smaller FOV images.

DISCUSSION

Two-dimensional Hadamard encoding offers the potential for acquiring images with high spatial resolution and large FOV. When screening tissue with high resolution, the region of interest need not be known a priori. The time needed to acquire a composite image with N tiles, is the same as required to acquire N separate high–resolution images with current limited FOV imaging schemes. However, as long as bandwidth per pixel remains constant the SNR of the Hadamard image will be $\sqrt{N}$ greater than that in each of the limited FOV images. Thus, if signal-to-noise is very high, the Hadamard approach seems to offer little; however when high resolution is needed, SNR drops and multiple acquisitions are needed, so in such situations the Hadamard approach does offer a significant time advantage over the conventional limited FOV approach. If, however, a priori knowledge of the region of interest exists, then the limited FOV technique is more advantageous. This is due to the fact that to properly encode the large FOV with an $N \times M$ Hadamard matrix, all encodings must be acquired regardless of which particular smaller region we would like to image.

There are various features of the sequence that must be carefully controlled when designing the sequence. 1) The region of the object lying in the transition bands are 'lost' as is clearly seen in the figures. Therefore, strong gradients must be used in conjunction with pulses having narrow transition bands to keep this lost information to a minimum; 2) The transition bands follow isocontours of frequency and therefore, the definition of the volumes is sensitive to B_o inhomogeneity and chemical shift. These effects can be minimized by using strong gradients during Hadamard encoding.

When used with a two-dimensional imaging sequence, the spatial encoding is performed using pre-encoding pulses so can in principle be used in conjunction with any two-dimensional imaging scheme. However, the pre-encoding section of the sequence must be kept short compared with the T_1 values of the tissue under observation to minimize the T_1 relaxation effect of the inverted spins. If there is significant relaxation, then the inverted spins will not have a signal that is $-1 \times$ the signal of the same spins when not inverted, and this is a requirement of the reconstruction.

We have demonstrated the ability to perform Hadamard encoding in the breast. In the clinical setting dynamic contrast agents are used to investigate breast lesions. At present, the Hadamard encoded images are acquired consecutively, so the component Hadamard images would not represent data from equivalent temporal points. One encoded image would have a different concentration of contrast than the other. Therefore for dynamic contrast studies, Hadamard imaging would require a protocol in which the acquisition for the component images are interleaved. This would ensure that both component images would represent data from equivalent time points.

In human studies, the most useful application may arise in situations where a researcher is interested in imaging several small objects within a larger FOV and may be advantageous in selectively increasing SNR for specific image regions without the need to acquire high image quality for the entire large FOV. In areas where localized motion may affect imaging such as coratid imaging, this technique may aid in ignoring the areas that are the cause of motion artifacts and focus directly on the high-resolution areas of interest. Much like the situation of multiple lesions within the breast, as long as the entire

large FOV is encoded with the appropriate matrix, the smaller objects of interest can easily be reconstructed.

Furthermore, The Hadamard technique may be employed in certain circumstances to increase the potential of some conventional clinical scanners. This would be due to the lack of suitable reconstruction algorithms or the data flow not being handled by the computer hardware in satisfactory time. This is accomplished through recombining the separate smaller sized images (that are easily handled by the hardware and algorithms) into the more computer intensive high-resolution images off-line on a separate workstation. Though limited in its scope, the Hadamard technique may be useful in high-resolution imaging. Between the advantages of off-line processing of larger data sets and the selective SNR increase in certain circumstances, this technique has definite applicability in clinical techniques.

Acknowledgments—We would like to thank Dr. Felix Wehrli and Dr. Mike Smith for their invaluable contributions to this body of work. This work was supported in part by a PHS grant from the National Institutes of Health, Division of Research Resources, P41-RR02305.

REFERENCES

1. Matthaei, D.; Frahm, J.; Haase, A.; Merboldt K.D.; Hanicke, W. Multipurpose NMR imaging using stimulated echoes. Magn. Reson. Med. 3:554–561; 1986.
2. Shungu, D.C.; Glickson, J.D. Sensitivity and localization enhancement in multinuclear in vivo NMR spectroscopy by outer volume suppression. Magn. Reson. Med. 30:661–671; 1993.
3. Bolinger, L.; Leigh, J.S. Hadamard spectroscopic imaging (HSI) for multi-volume localization. J. Magn. Reson. 80: 162–167; 1988.
4. Goelman, G.; Walter, G.; Leigh, J.S. Hadamard spectroscopic imaging technique as applied to study of human calf muscles. Magn. Reson. Med. 25:349–354; 1992.
5. Vanderborne, K.; Walter, G.; Leigh, J.S.; Goelman, G. pH heterogeniety during exercise in localized spectra from single human muscle. Am. J. Physiol. 265:C1332–C1339; 1993.
6. Goelman, G. Fast Hadamard spectroscopic imaging techniques. J. Magn. Reson. Series B 104:212–218; 1994.
7. Dreher, W.; Leibfritz, D. Double-echo multi-slice proton spectroscopic imaging using Hadamard slice encoding. Magn. Reson. Med. 31:596–600; 1994.
8. Gonen, O.; Hu, J.; Stoyanovc, R.; Leigh, J.S.; Goelman, G.; Brown, T.R. Hybrid three dimensional (1D-Hadamard, 2D chemical shift imaging) phosphorus localized spectroscopy of phantom and human brain. Magn. Reson. Med. 33:300–308; 1995.
9. Maudsley, A.A. Multiple-line scanning spin density imaging. J. Magn. Reson. 41:112–126; 1980.
10. Souza, S.P.; Szumowski, J.; Dumoulin, C.L.; Plewes, D.D.; Glover, G. SIMA: Simultaneous multi-slice acquisition of MR images by Hadamard-encoded excitation. J. Comp. Assist. Tomogr. 12:1026–1030; 1988.
11. Bolinger, L.; Prammer, M.G.; Leigh, J.S. A multiple frequency coil with a highly uniform B_1 field. J. Magn. Reson. 81:162–166; 1989.
12. Shinnar, M.; Eleff, S.; Subramanian, H.; Leigh, J.S. The synthesis of pulse sequences yielding arbitrary magnetization vectors. Magn. Reson. Med. 12:74–80; 1989.
13. Shinnar, M.; Bolinger, L.; Leigh, J.S. The use of finite impulse response filters in pulse design. Magn. Reson. Med. 12:81–87; 1989.
14. Shinnar, M.; Bolinger, L. Leigh, J.S. The synthesis of soft pulses with a specified frequency response. Magn. Reson. Med. 12:88–92; 1989.
15. Silver, M.S.; Joseph, R.I.; Hoult, D.I. Highly selective p/2 and p pulse generation. J. Magn. Reson. 59:347–351; 1984.
16. Silver, M.S.; Joseph, R.I.; Hoult, D.I. Selective spin inversion in nuclear magnetic resonance and coherent optics through an exact solution of the Bloch–Riccati equation. Phys. Rev. A. 31:2753–2755; 1985.
17. Goelman, G.; Subramanian, V.H.; Leigh, J.S., Transverse Hadamard spectroscopic imaging technique. J. Magn. Reson. 89:437–454; 1990.
18. Roberts, D.A.; Insko, E.K.; Bolinger, L.; Leigh, J.S. Biplanar radiofrequency coil design. J. Magn. Reson. Series A. 102:34–41; 1993.
19. Insko, E.K.; Bolinger, L. Mapping of the radiofrequency field. J. Magn. Reson. Series A 1993;103:82–85.